www.czasopisma.pan.pl PAN POLSKA AKADEMIA NAUK www.journals.pan.pl

Arch. Metall. Mater. **66** (2021), 2, 617-626

DOI: 10.24425/amm.2021.135899

S. SARAVANAKUMAR[1*], S. GOPALAKRISHNAN[2], K. KALAISELVAN[3]

DEVELOPMENT OF EMPIRICAL RELATIONSHIPS FOR PREDICTION OF MECHANICAL AND WEAR BEHAVIOR OF COPPER MATRIX SURFACE COMPOSITE BY FRICTION STIR PROCESSING TECHNIQUE

In this investigation, Copper Matrix Surface Composites (CMSCs) were reinforced with various ceramic particles like Aluminum Nitrate (AlN), Titanium diboride (TiB_2), and Rice Husk Ash (RHA) are used to increase the metallurgical and mechanical properties by Friction Stir Processing (FSP). The Design of the Experiment (DOE) Taguchi L_9 orthogonal array method was used. The process parameters considered were groove width and various types of reinforcement particles. The fabrication of CMSCs was achieved by using optimized process parameters, such as the tool transverse speed of 40 mm/min, rotational tool speed of 1000 rpm, and an axial load of 10 kN with one pass. The influence of FSP process parameters on CMSCs in the stir zone is observed through Optical Microscope (OM), Field Emission Scanning Electron Microscope (FESEM), and Transmission Electron Microscope (TEM). Mechanical properties such as microhardness and wear rate are studied and compared. It reveals that good interfacial bonding was produced between ceramic particles in CMSCs. TiB_2 reinforced with copper matrix surface composites enhance microhardness and had a lesser wear rate.

Keywords: Friction stir processing, Microstructure, Microhardness, Wear

1. Introduction

Copper is mostly considered for thermal and electrical conduction. Its superior properties of ductility, high resistance to corrosion and oxidation led to easy fabrication. Because of those characteristics, copper has high attention from various manufacturing industries. It is not restricted to optical, electrical, and thermal industries [1,2]. Some limitations of copper are low mechanical strength, low hardness, and less wear resistance. These properties need enhancement for particular applications, for example, electrical contact breakers, nozzles, and bearing bushes, etc. These properties may be improved in heat treatment [3], alloying [4], dispersion strengthening [5], and plastic deformation [6].

Strengthening of copper through dispersion reinforcement particles is widely accepted. These particles are reinforced into the copper matrix known as Copper Matrix Composites (CMC). Some CMC materials are required to increase hardness and wear resistance without significant degradation of the electrical and thermal conductivity of the copper [7]. The ceramic particle's different types, for example, TiC [8], SiC [9], Al_2O_3 [10], and WC [11] are utilized by way of reinforcements for fabricating CMC. The selection of reinforcement is RHA as a cultivation waste. This is available in large amounts of quantity in India, Brazil, and China. Aluminum-based composites reinforced with RHA particles were improved their properties [12,13]. Hence, Aluminium Nitrate (AlN) is the right choice for the selection of reinforcement to fabricate CMSC, particularly in electrical and electronic industry applications. It also has good thermal and electrical conductivities. It has a low coefficient of thermal expansion, high dielectric constant, and chemical stability [14,15]. Producing Cu/AlN composites will increase the wear resistance, besides decreasing the piling of thermal stress in electrical and electronic machinery types. A very few investigators reported that Cu/AlN properties are improved by the methods of mechanical alloying [16], hot pressing [17], pressure infiltration [18], vacuum infiltration [19], gas, and reactive infiltration [20], etc. The selection of TiB_2 reinforcement is a most traditional ceramic material that keeps a suitable combination of mechanical and physical properties, such as fairly melting high temperature, good electrical conductivity, high hardness, and elastic modulus. Hence, TiB_2 particles enhance properties for copper matrix composites. Currently, CMC was produced utilizing a wide range of liquid metallurgy and solid-state methods. The production techniques as follows: powder metallurgy process

[1] DEPARTMENT OF MECHANICAL ENGINEERING, M. KUMARASAMY COLLEGE OF ENGINEERING, KARUR, TAMILNADU, INDIA
[2] DEPARTMENT OF MECHANICAL ENGINEERING, KS RANGASAMY COLLEGE OF TECHNOLOGY, TIRUCHENGODE, TAMILNADU, INDIA
[3] DEPARTMENT OF MECHANICAL ENGINEERING, DR. NGP INSTITUTE OF TECHNOLOGY, COIMBATORE, TAMILNADU, INDIA

* Corresponding author: saravananmeksr@gmail.com

[21] mechanical alloying process [22], the hot pressing process [23], spark plasma sintering [24], laser melting process [25], stir casting process [26], squeeze casting method [27], pressure less infiltration [28], combustion synthesis [29] and spray forming method [30]. It is tough to produce with greater properties CMCs. There are various types of defects such as porosity, cluster formation, and non-uniform dispersion, grain boundaries along with segregation, interfacial bonding reactions in the matrix material, and reinforcing particles that occur in CMCs. Many investigators have analyzed parameters using central composite design in friction stir welding. Empirical relationships were generated to predict the mechanical properties of CMCs by statistical analysis.

FSP technique was used to fabricate Metal Matrix Surface Composites (MMSC) recently [31]. The FSP working principle depends upon Friction Stir Welding (FSW) [32]. The hybrid mixture of advanced ceramic particles dependent on nitride (25% AlN + 75% BN) was spread via the FSP technique on the copper matrix surface at various volume fractions. The effects revealed an increase in mechanical characteristics to the increased particle dispersion [33]. FSP is a thermo-mechanical process that combines the production of composites with the processing of plastic deformation and frictional heat. Thus, the main scope of this investigation was to produce Cu/AlN, Cu/TiB_2, and Cu/RHA composites as well as evaluate the microstructural characteristics in addition to microhardness and sliding wear behavior of the CMSCs.

2. Experimental procedure

2.1. Process parameters identification

The CMSCs are influenced by FSP parameters of the groove width (W), and ceramic particle type (C) are significant influences the material properties.

2.2. Limits of the FSP parameters

The operating range of every process parameter is identified and fixed at different trial runs. In the friction stir processing specimens, defects such as wormhole, pinhole, tunnel, etc., were minimized. FSP area is restricted for many defects based on the chosen limits of each factor. The limits to be coded as –1, 0, +1 the factors lower and higher are used respectively to prepare the experimental data. Process parameters are listed in Table 1 for selected levels using their units and notations.

TABLE 1

Process parameters and their levels

Sl No	Process Parameter	Notation	Levels		
			–1	0	1
1	Width of the groove	W	0.4	0.8	1.2
2	Ceramic particle	C	AlN	TiB_2	RHA

2.3. Developing a design matrix

The Taguchi method is well-established for the development of optimizing product design or fabricating processes. It is used to develop the processing and machining parameters of manufacturing industries such as casting, forging, forming, and welding. A full factorial experimental design is attention to overall performance characteristics. These strategies utilized are adopted to decide the two response problems effectively. In this investigation, the determination of process parameters based on these two responses to be improved of CMSC given in Table 2.

TABLE 2

Design matrix using its experimental results

Experiment No.	Design matrix		Experimental		Width of the groove (mm)	Micro hardness (HV)	Wear rate (X 10^{-5} mm^3/m)
	C	W	C	W			
1	–1	–1	AlN	0.4	0.4	78.2	211
2	–1	0	AlN	0.8	0.8	90.1	198
3	–1	1	AlN	1.2	1.2	109.4	175
4	0	–1	TiB_2	0.4	0.4	98.1	171
5	0	0	TiB_2	0.8	0.8	108.2	161
6	0	1	TiB_2	1.2	1.2	128.3	141
7	+1	–1	RHA	0.4	0.4	79.4	210
8	+1	0	RHA	0.8	0.8	101.4	180
9	+1	1	RHA	1.2	1.2	116.2	160

2.4. Production of CMSCs as per the design matrix

Pure copper, normally known as electrolytic copper, is the base metal. Chosen plates for the experimental analysis as per the dimensions 100 × 50 × 10 mm as displayed in Fig. 1. Table 3 presents the chemical composition of pure copper. The reinforcement particles such as AlN, TiB_2, and RHA were chosen for surface modification of the copper material. The ceramic particles used for the experimentation confirmed with SEM

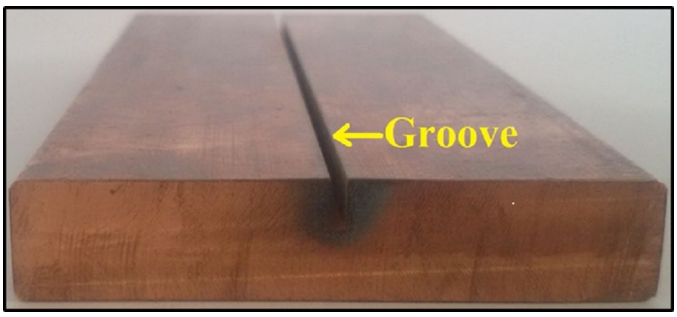

Fig. 1. Grooved copper base metal

TABLE 3

Composition of copper metal

Element	Zn	Al	Fe	Ni	Mg	Si	C	Pb	Cu
% wt.	0.04	0.19	0.007	0.004	0.002	0.04	0.02	0.005	99.7

micrograph, and it is shown in Fig. 2 a size of groove depth 4 mm and 0.4, 0.8, and 1.2 mm width was prepared in the center of the copper plate by wire-cut EDM and packed the particles with 6, 12, and 18% of volume fraction. A double tempered H13 steel tool with pin fabricated as presented in Fig. 3 a pinless tool used on the surface of the grooved plates to close it. This method avoids the spreading of reinforcement particles on the outer surface of the machined groove during the stirring action. The

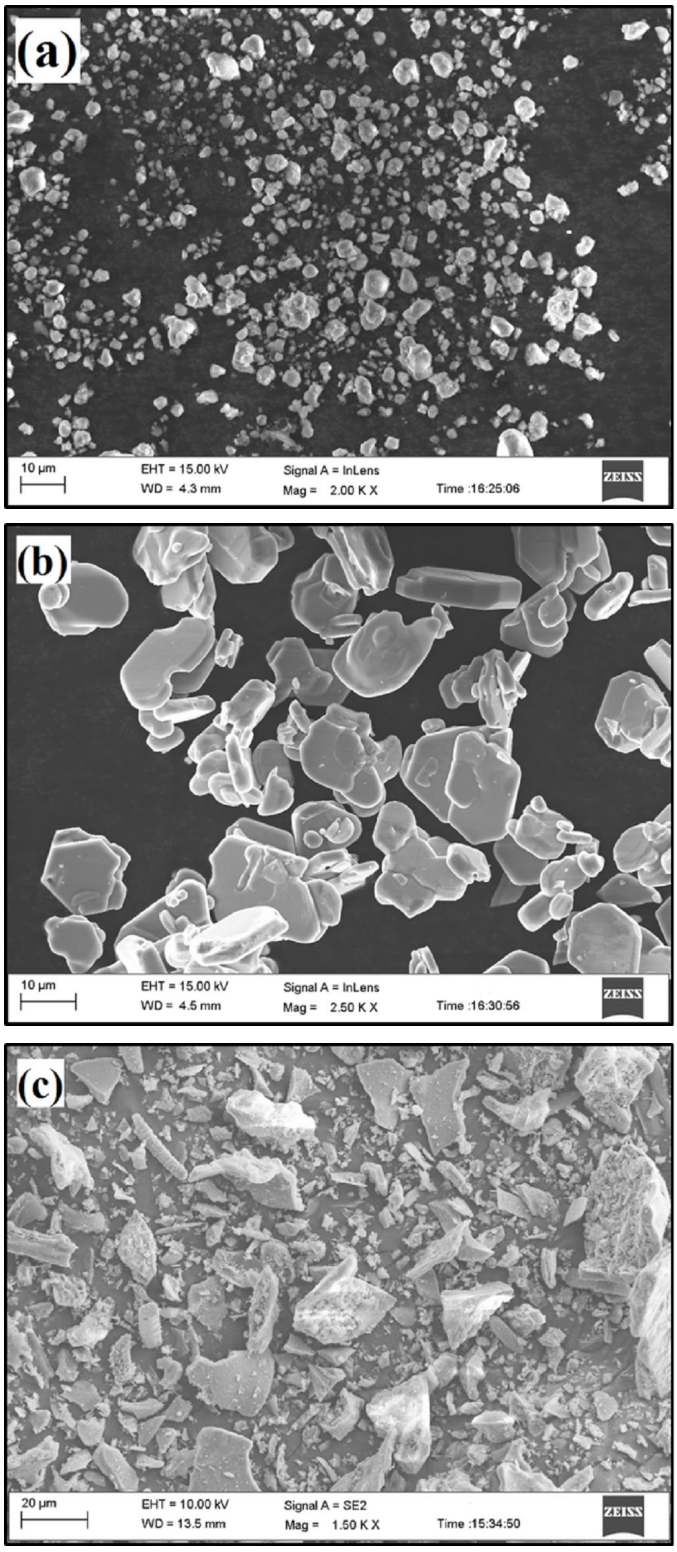

Fig. 2. FESEM of ceramic particles (a) AlN, (b) TiB_2, and (c) RHA

FSP machine process parameters are 1000 rpm tool rotational speed, 40 mm/min transverse speed in addition to10 kN an axial load was used with one pass without any tilt. FSP experiments were completed as per the design matrix. The plates processed for the FSP are seen in Fig. 4(a) Cu/AlN, (b) Cu/TiB_2, and (c) Cu/RHA, respectively.

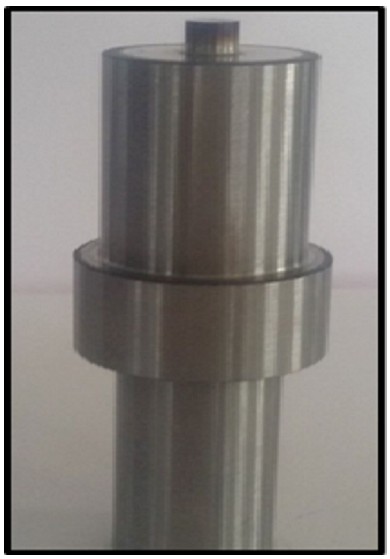

Fig. 3. Friction stir processing tool

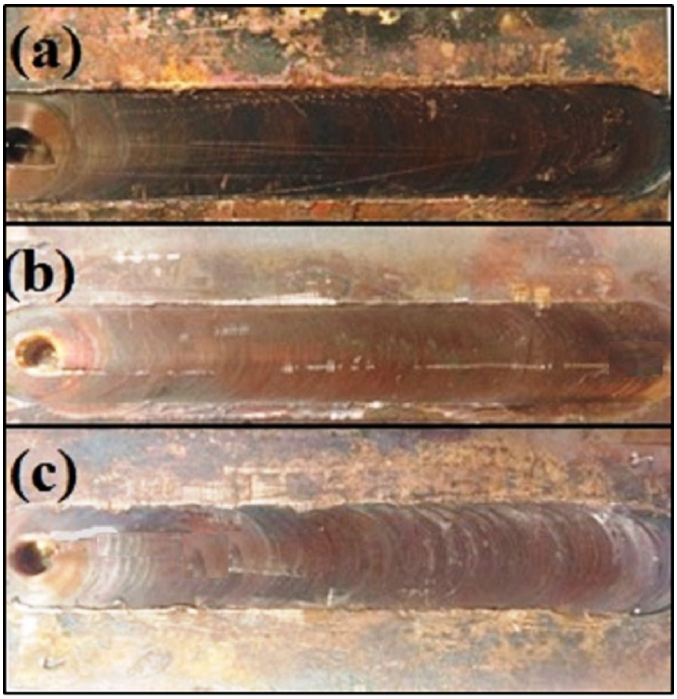

Fig. 4. The crown appearance of the friction stir processed plates (a) Cu/AlN, (b) Cu/ TiB_2, and (c) Cu/ RHA

2.5. Recording the response parameters

The samples were machined to evaluate the microstructure, microhardness, and wear rate of the composites. The CMSC samples were polished with 20 grams of chromic acid, 2 grams

of sodium sulfate and 1.7 ml of HCl in 100 ml of distilled water by metallographic standards and color etched for a given period of 10 seconds. Using an optical scanner, the digital image of the etched specimen's macrostructure was captured. An OM and FESEM take the micrographs. Copper matrix surface composite microhardness was measured around the cross-section perpendicular to the process direction at different locations at a load of 500 g applied in the stir zone for 15 seconds. The wear characteristic of CMSCs was measured by employing a pin-on-disc wear apparatus without lubrication at ambient temperature at the size of the pin 4 × 6 × 20 mm was used. Wear parameters such as load 30 N, sliding disc velocity is 1.5 m/s, and 3000 m sliding distance was used.

2.6. Development of empirical relationships

The process parameters' functions are groove width and reinforcement particles, which are referred to as Eq. (1).

$$Y = f(C, W) \tag{1}$$

The selection of the polynomial equation for expressed all responses Eq. (2).

$$Y = b_0 + b_1 W + b_2 C + b_{11} W_2 + b_{22} C_2 + b_{12} WC \tag{2}$$

Where the average response is b_0, and response coefficients are b_1, b_2, b_{11}, b_{22}, and b_{12} based on the effect of selection parameters. The coefficients are resolved by the utilization tool of MINITAB 16 Software. The mathematical models were developed while finding out the coefficients, and it was observed that the coefficient's confidence level was at 95%. The irrelevant coefficients are disposed of without disturbing the precision of the mathematical models and utilizing the understudy of the F-test. The mathematical models created with FSP processing factors encoded for the responses are statistical results of the regression models in Eq. (3) and Eq. (4)

Microhardness = 101.06 – 8.49 reinforcement AlN + 10.48 reinforcement_TiB_2 – 1.99 reinforcement_RHA – 15.82 groove width_0.4 – 1.16 groove width_0.8 + 16.98 groove width_1.2 (3)

Wear Rate = 178.56 + 16.11 reinforcement_AlN – 20.89 reinforcement_TiB^2 + 4.78 reinforcement_RHA + 18.78 groove width_0.4 + 1.11 groove width_0.8 – 19.89 groove width_1.2 (4)

2.7. Checking empirical relationships

The statistical significance of the empirical relationships is formed as given in Table 4. The expected values are closely equal, and the R-square value is 1 of the experimental result. R-square expression reveals accepted empirical relationships. This is used to investigate all responses to the analysis of variance (ANOVA) method, which is detailed in Table 5 at a confidence level of 95%; the assessment of the F ratio is calculated it is higher than that of the tabulated values. Also, the scatter diagrams in Fig. 5(a) show that a larger S-N ratio gives better results for hardness, and Fig. 5(b) shows that a lower S-N ratio gives better results for wear rate. Thus, the proven empirical relationships are sufficiently adequate.

TABLE 4

Statistical outcome results of the regression model

Response	R-Square	Adjusted R-Square	Standard Error
Microhardness	0.98	0.96	0.02
Wear rate	0.96	0.93	0.03

TABLE 5

ANOVA Consequences of the developed mathematical models

S. No	Response	Source	Sum of Squares	Degrees of freedom	Mean square	F-Ratio
1	Micro-hardness	Regression	1619.77	2	809.88	26.91
		Residual	557.4	2	278.88	
2	Wear rate	Regression	2154.2	2	1078.11	28.79
		Residual	2248.2	2		

2.8. Validation of empirical relations

To validate the developed empirical relationships, conformity tests were done. The evaluations completed at exceptional values of groove width and types of ceramic particles are measured in their response and design matrix. The results error in the prediction to be considered error percentage within ±5%, the developed empirical relationships accuracy confirms with displayed in Table 6.

Error percentage = [(Measured value-Predicted value) / Predicted value] × 100

TABLE 6

Conformity experiments results

Trial Run	FSP parameter		Microhardness (HV)			Wear rate X 10^{-5} mm^3/m		
	W	C	Actual value	Predicted value	Error (%)	Actual value	Predicted value	Percentage of Error (%)
1	0.4	TiB_2	98.1	96.76	1.34	171	175.4	4.4
2	0.8	AlN	90.1	92.23	2.13	198	194.6	3.4
3	1.2	RHA	116.2	114.33	1.87	160	164.4	4.4
Average					**1.78**			**4.06**

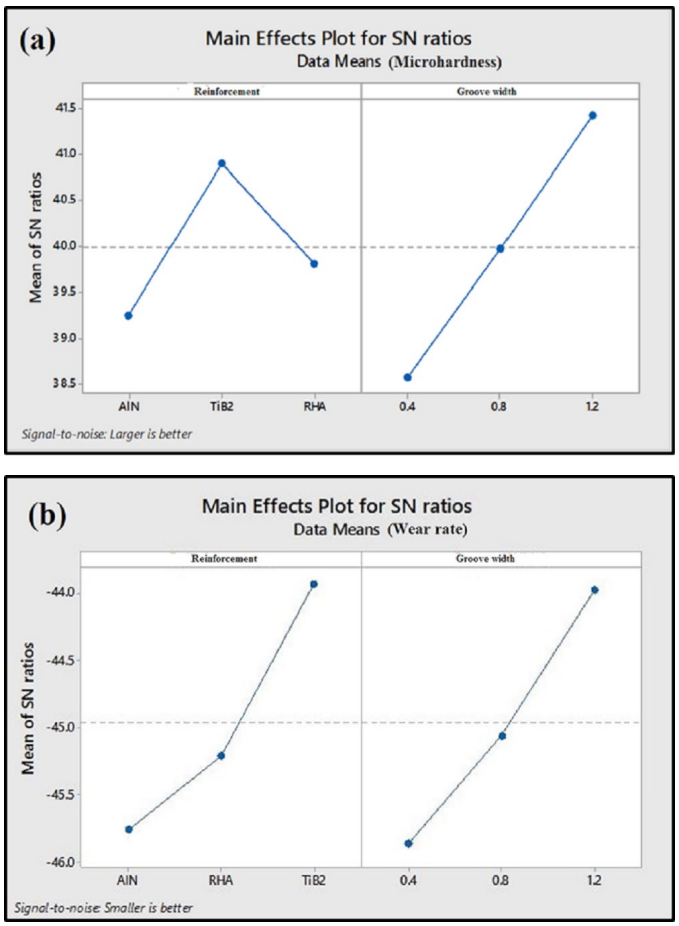

Fig. 5. Scatter diagram of (a) microhardness (b) wear rate

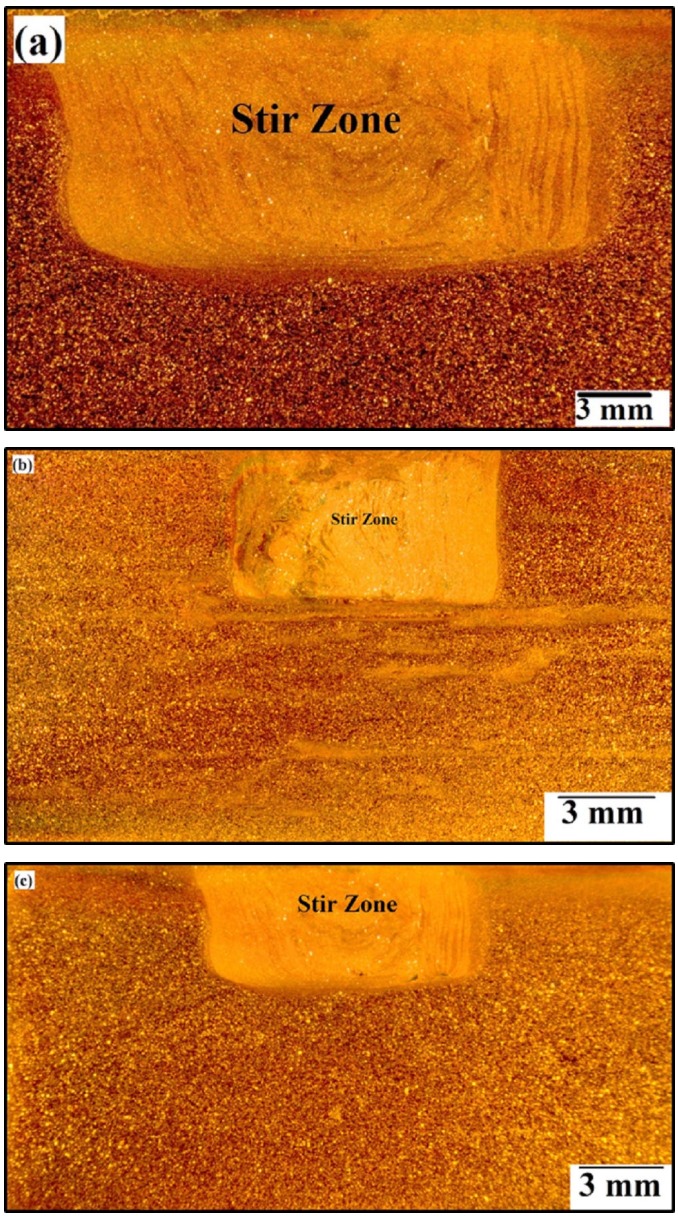

Fig. 6. Macrostructure of stir zone (a) Cu/AlN, (b) Cu/TiB_2, and (c) Cu/RHA

3. Results and discussion

The effect of groove width and type of ceramic particle on the stir zone area of the CMSCs. The microhardness and wear rate has been predicted from the established empirical relationships. The subsequent sections are to understand the possible reasons for the achieved results and compare the microstructure and mechanical properties of the CMSCs.

3.1. Macrostructure of CMSCs

Fig. 6 (a) Cu/AlN, (b) Cu/TiB_2, and (c) Cu/ RHA illustrates macrostructure for CMSCs, which has an area of stir zone seen in defect-free. With the full formation of copper matrix composite and duration, the FSP materials are plasticized, and continuous flow is visible. The heat is produced by the shearing of the pin and friction of the tool shoulder. The macrostructure reveals that reinforcement particles mixed properly with plasticized copper, and the CMSCs formed. The plasticized material is formed as the complete consolidation, and it is called the stirred area [34]. The width of the stir zone is more than the diameter of the pin. Several factors, including the use of reduced travel speeds, can be attributed to the change. Copper has high thermal conductivity, which induces frictional heat distribution in the lateral direction and the progress in the copper deformation of additional frictional heat. The presence of reinforcement particles may have filled the entire region.

3.2. Microstructural characterization

3.2.1. Optical microstructure

The pure copper optical microstructure is presented in Fig. 7 the microstructure of CMSCs fabricated by FSP is clearly illustrated in Fig. 8 (a) Cu/AlN, (b) Cu/TiB_2, and (c) Cu/RHA. The stir zone confirms that the grains are very fine when compared to the copper matrix. This grain surface reduces the influence of plastic deformation along with the heat generated in the workpiece during the stirring process, the action leading to undergo recrystal-

lization. The grain size of ceramic particle variation during FSP is categorized by two states; the first states that during FSP fine grain size is attained that generation of frictional heat. Second one state that the reduced size of grain mostly happens by stirring action constantly. It is noticeable that the grain size of the CMSCs is very finer it was observed and compared with the copper.

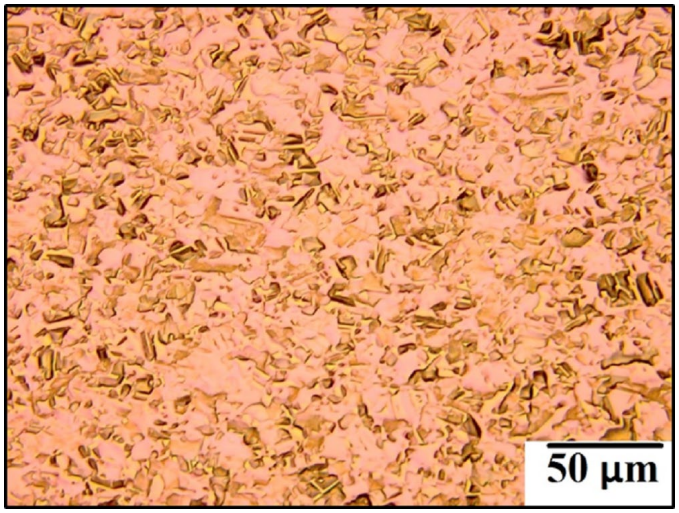

Fig. 7. Micrograph of pure copper

3.2.2. FESEM microstructure

Fig. 9 (a) Cu/AlN, (b) Cu/TiB_2, and (c) Cu/RHA presents the distribution of the particles inside the stir zone is revealed by FESEM micrographs. The distributions of ceramic particles are notified and are homogeneous. There is not even any cluster identified, the grain boundaries of particles segregated. The distribution of particles intra-granular and homogeneous is desired to attained superior properties of composites. These FESEM micrographs obtained in particles are distributed properly with the matrix material. In this work, the optimized process parameters are carefully chosen to fabricate the CMSCs to achieve homogeneous and intragranular particle distribution. The FSP tool made by dynamic stirring action is used to knock off sharp corners of particles.

Fig. 10 (a) Cu/AlN, (b) Cu/TiB_2, and (c) Cu/RHA depict the higher magnification of the SEM micrographs; it is shown that there is no clustering of minor debris either seen. The good interfacial bonding and uniform distribution of the ceramic particles are attributed to sufficient frictional heat generation, optimized tool action, and plasticized material flow in the stir zone [35].

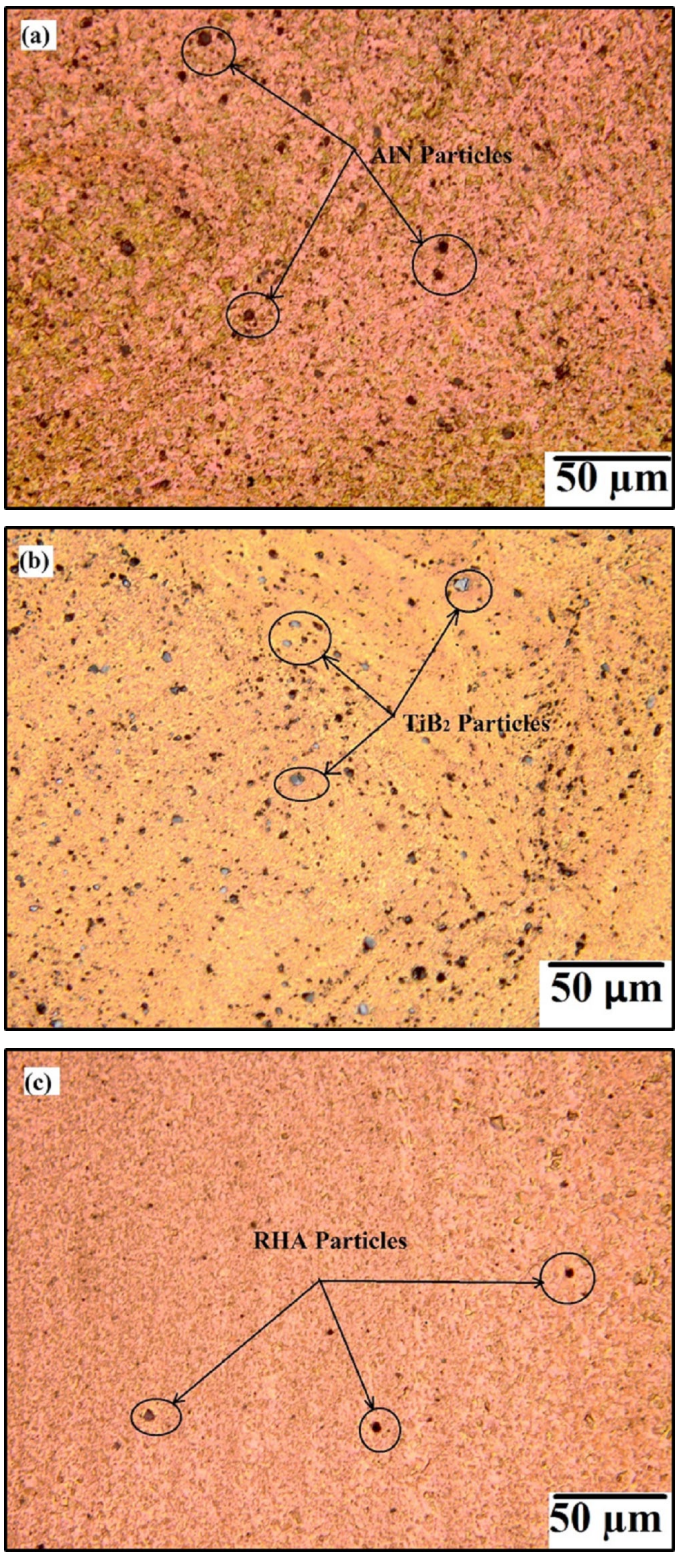

Fig. 8. Optical photomicrograph of CMSCs (a) Cu/AlN, (b) Cu/TiB_2, and (c) Cu/RHA

3.2.3. Transmission electron microscopy images

Cu/AlN is presented as TEM images in Fig. 11 the images reveal in the grain structure are very fine besides high dislocation density. This dislocation density performs being low within the grain areas. The reason may be accredited to discontinuous dynamic recrystallization. The maximum quantity of dislocations may be recognized as the subsequent causes. Metal is deeply deformed to produce the composite. AlN particles are not equivalent to the thermal properties of the copper matrix. The enlargement and reduction of both materials are not similar. Therefore, additional dislocations are formed to accommodate to mismatch the thermal properties. TEM image expressions show the presence of annealing twins. Cu/TiB_2 composite TEM images

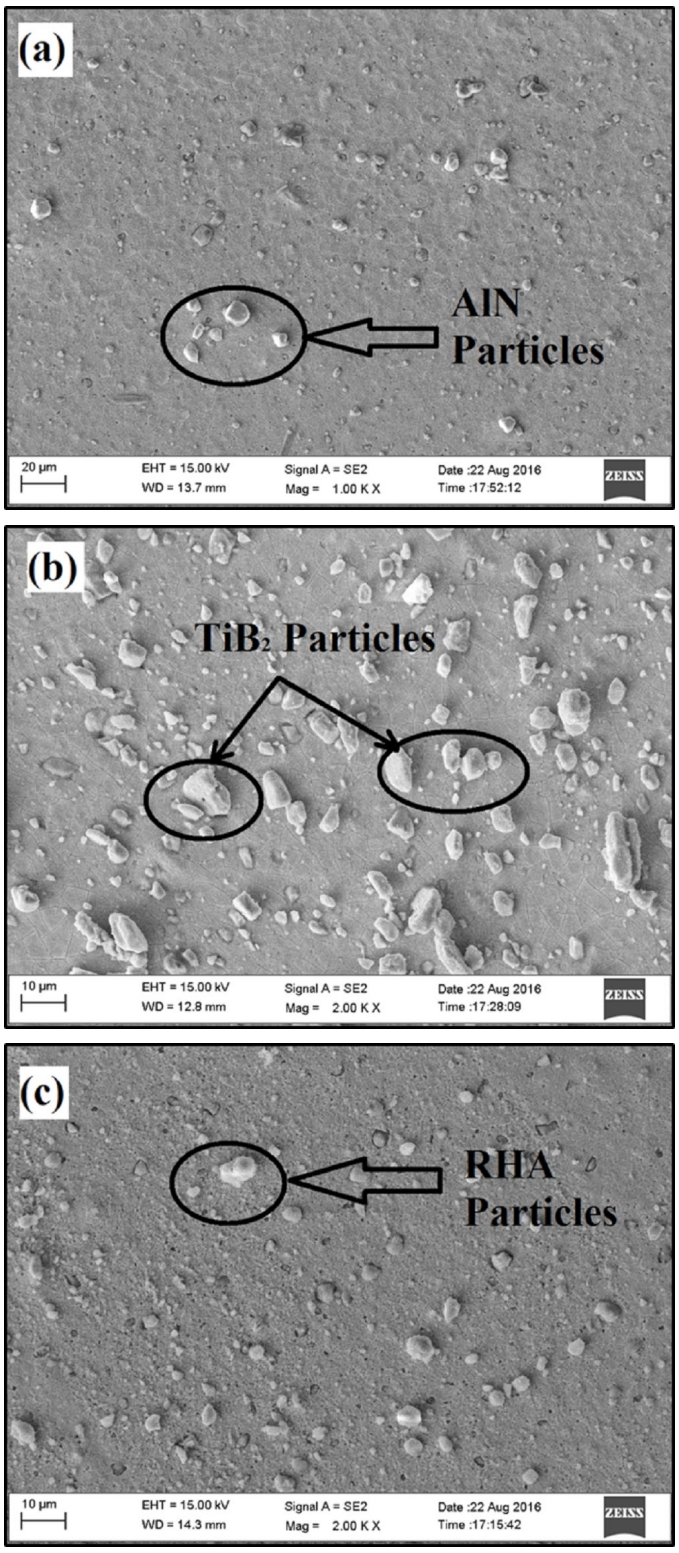

Fig. 9. FESEM micrograph CMSCs reinforced with: (a) AlN, (b) TiB_2, and (c) RHA

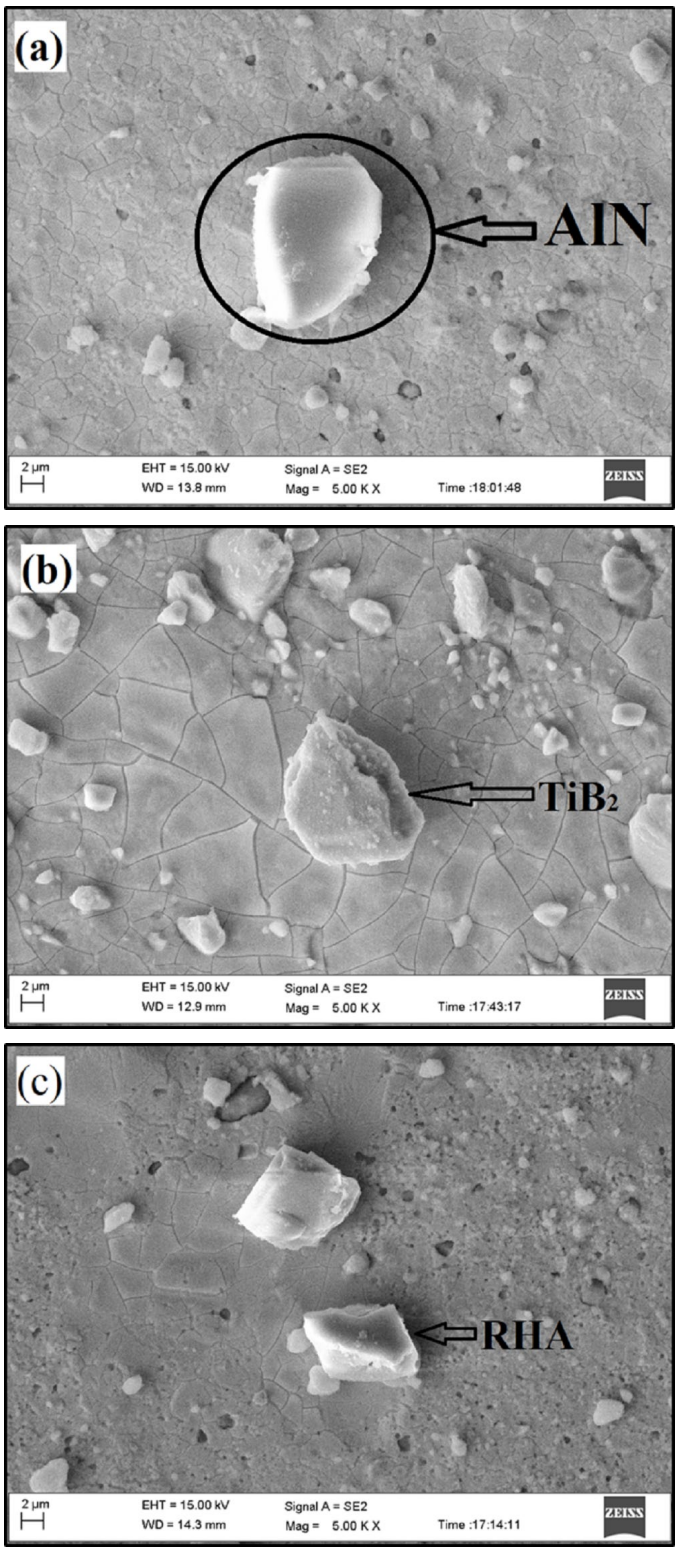

Fig. 10. FESEM micrograph CMSCs at higher magnification (a) Cu/AlN, (b) Cu/TiB_2, and (c) Cu/RHA

are shown in Fig. 12. It reveals that stimulating to notice ultra fine grains present maximum dislocation density. In the inner grain boundaries, minimum dislocation density is noticed. This influence is a dynamic recrystallization process and this high dislocation density effect is the following factors. Dislocations create while the material is exposed to deformation, and recrystallized grains are frequently deformations. Also, the thermal mismatch between the TiB_2 particles and copper creates extra dislocations in the composites [36]. The micrographs notice the dislocations and pinned grain boundaries then the TiB_2 particles are subsidized to the Zener-pinning effect. Cu/RHA composite for TEM images are shown in Fig. 13 it reveals that ultrafine

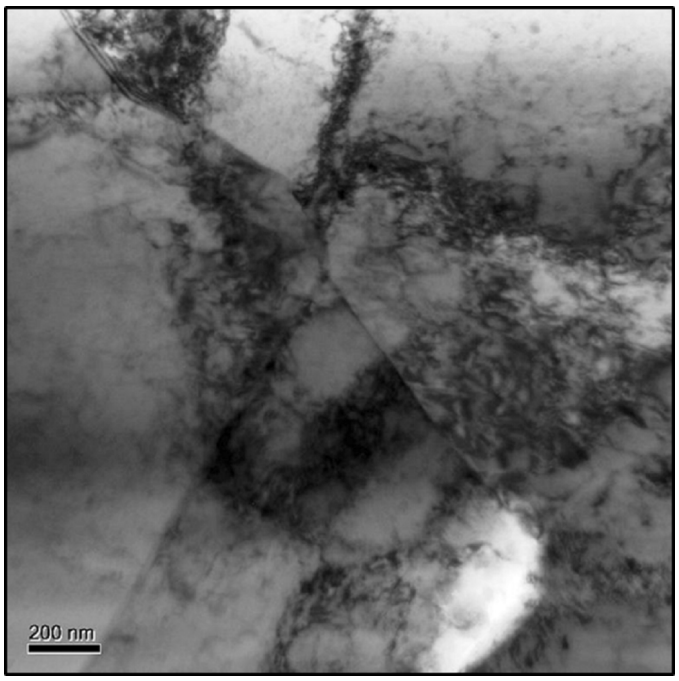

Fig. 11. TEM image of Cu/AlN CMSCs

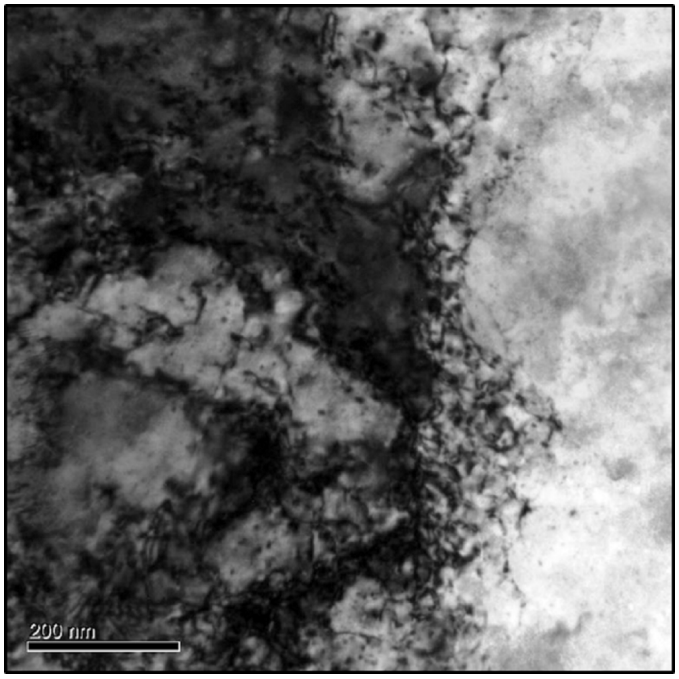

Fig. 12. TEM image of Cu/TiB_2 CMSCs

grains are just as maximum dislocation density. The inside areas of certain grains are plain and it shows the minimum dislocation density. The interface of the copper and RHA can be identified. The particle is not surrounded by a process layer.

3.3. Microhardness of CMSCs

CMSCs microhardness of Cu/AlN, Cu/TiB_2, and Cu/RHA are shown in Table 2. The microhardness of pure copper is 64 HV.

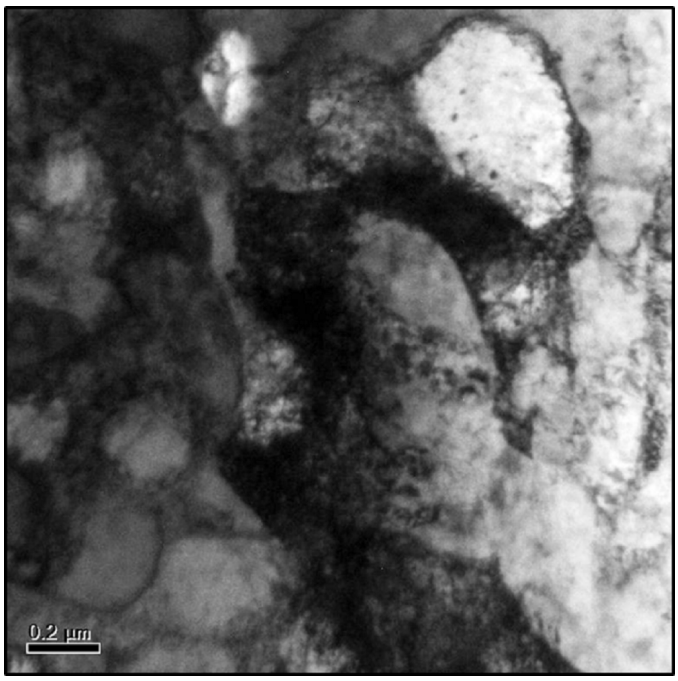

Fig. 13. TEM image of Cu/RHA CMSCs

CMSCs upgrade the microhardness value above the base metal. The Cu/TiB_2 attains a microhardness value of 128.3 HV. Fig. 14 describes that when compared to the copper, the hardness value has been increased in the friction stir zone very well. The factors are as follows: (i) high hardness of ceramic particles (ii) grain size particle reduction as an outcome of dynamic recrystallization (iii) particle grain size and (iv) quench hardening effect that thermal condensation variations occur after-effect between particles and base materials [37]. Ceramic particles of dispersion uniformly in the stir zone aspects, the reason for an increment of hardness. The FSP leads to be very high in dynamic recrystallization in that way fine grain size of CMSCs. The grains refined contribute to improving the hardness of the material. The CMSC's mechanical properties are mostly influenced through shape, size, volume fraction, and types of reinforcement particles revealed a homogeneous distribution within the copper matrix.

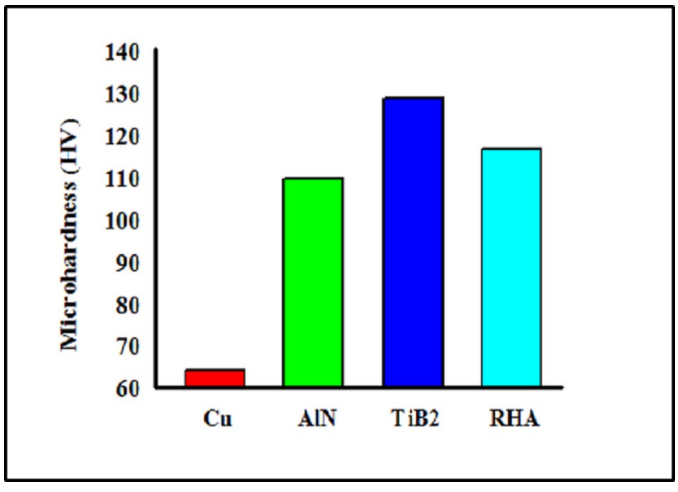

Fig. 14. Effect of reinforcement on microhardness

The nonappearance of porosity and clusters confirms the minimum difference of the hardness. Negligible shape variation of the ceramic particle to be considered. The particles are noticed irregular polygonal shapes. Present experimental work shows the increased microhardness value concerning the selection of reinforcement because of dynamic recrystallization and uniform distribution of particles. The Cu/TiB_2 hardness value is higher than compared to Cu/AlN and Cu/RHA.

3.4. Sliding wear behavior of CMSCs

CMSCs wear rate of Cu/AlN, Cu/TiB_2, and Cu/RHA are present in Table 2. The wear rate of pure copper is estimated as 248×10^{-5} mm^3/m using pin-on-disc wear test apparatus. Combination with copper and ceramic particles enhanced wear rate is lower than the base metal of the copper the wear test specimens of size $4 \times 6 \times 20$ mm are given in Fig. 15. Cu/TiB_2 reveals a minimum of 141×10^{-5} mm^3/m wear rate, as shown in Fig. 16. The result shows that adding ceramic particles to CMSCs improves wear resistance significantly. Archard's wear law state the relationship between wear rate and hardness [38]. While the material hardness is higher, and the wear rate will be lower. The hardness improvement is based on ceramic particle distribution and grain refinement for improvement to wear rate resistance. Scopes of CMSCs are upgraded with great hardness, also, to wear-resistant properties for selection of copper. By the statement, CMSCs with varying ceramic particles exhibits wear rate is lower while compared with the base metal. Increases in ceramic particles dispersion, the wear rate tends to decrease generally caused by (i) ceramic particles distribution uniformly into copper matrix (ii) hardness of CMSCs is upgraded (iii) reduction in the surface of the copper matrix contact to rotating steel the particles to transfer the load away hence, highly reducing wear rate [39-40]. The other factors for reducing wear rate, particle grain size reductions that happen through the FSP, Copper being formable and ductile properties when contact with steel disc metal takes on plastic deformation that is called adhesion wear. The base metal undertakes both wear of abrasive and adhesion. Thus the ceramic reinforcement into the copper matrix decreases the material ductility and reduces the plastic deformation. The increase of microhardness value on the surface composite leads to the reduction of the metal removal rate for the duration of sliding wear. It reveals that the ceramic particles are a great benefit to decrease the wear rate of CMSCs.

Fig. 15. Wear test specimens

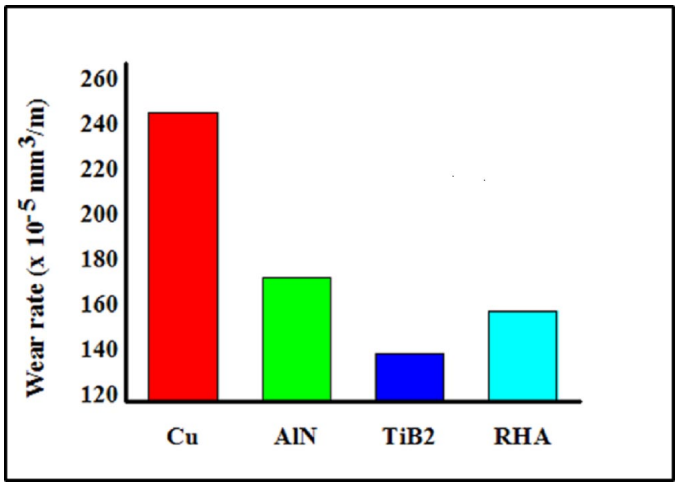

Fig. 16. Effect of reinforcement on the wear rate

4. Conclusion

Copper matrix with AlN, TiB_2, and RHA surface composites was effectively fabricated through the FSP technique. The CMSCs observe microstructure; the mechanical properties of hardness and sliding wear behavior were assessed. The present investigations concluded as follows:

- The grain size refined in the friction stir processed copper matrix surface composites was observed. It has a finer while compared with the base metal.
- SEM results revealed that the existence of ceramic particles in the copper matrix as well as confirming great interfacial bonding.
- During FSP, ceramic particle's shape and size did not change due to their minimum size smooth surface. Unproduced pores or interface reactions are observed in ceramic particles while bonding appropriately with the copper matrix.
- The CMSCs deviation in stir zone, particle grain size, hardness, and sliding wear rate are within the short-range.

Nevertheless, the Cu/TiB_2 exhibited higher hardness and resistance to wear rate compared to other CMSCs. This work Cu/X (X= AlN, TiB_2, and RHA) produced a set of optimized process parameters. In order to increase the microhardness, enhancement in wear resistance was correlated.

- FSP technique is suitable for fabricating CMSCs reinforced with various ceramic particles attained desirable properties.

REFERENCES

[1] S.C. Vettivel, N. Selvakumar, R. Narayanasamy, N. Leema, Mater. Des. **50**, 977-96 (2013). doi: https://doi.org/10.1016/j.matdes.2013.03.072

[2] A. Das, V. Verma, C.B. Basak, Mater. Charact. **120**, 152-58 (2016). doi: https://doi.org/10.1016/j.matchar.2016.08.021

[3] M.J. Dianez, E. Donoso, M.J. Sayagues, A. Perejon, P.E. Sanchez-Jimenez, L.A. Perez **688**, 288-294 (2016).

[4] Maqueda, Criado J. Alloys Compd. **688**, 288-94 (2016). doi: https://doi.org/10.1016/j.jallcom.2016.07.021

[5] Y. Champion, J. Bourgon, X. Sauvage, Mater. Sci. Eng. A, **657**, 1-5 (2016).

[6] M. Guo, L. Yi, J. Zhu, T. Lin, M. Li, Mater. Charact. **120**, 109-14 (2016).

[7] A. Uniwersal, M. Wrobel, K. Wierzbanowski, S. Wronski, M. Wronsk, I. Kalemba-Rec, Bacroix B, Mater. Charact. **118**, 575-83 (2016). doi: https://doi.org/10.1016/j.matchar.2016.07.004

[8] R.G. Zheng, Z.J. Zhan, W.K. Wang, Wear **268** (1-2), 72-76 (2010). doi: https://doi.org/10.1016/j.wear.2009.06.026

[9] S. Rathod, O.P. Modi, B.K. Prasad, A. Chrysanthou, D. Vallauri, V.P. Deshmukh, A.K. Shah, Mater. Sci. Eng. A, **502** (1-2), 91-98, (2009). doi: https://doi.org/10.1016/j.msea.2008.10.002

[10] G.C. Efe, M. Ipek, S. Zeytin, C. Bindal, Com. Part B: Eng. **43**, 1813-22 (2012).

[11] A. Fathy, A.A. Megahed, Int. J. Adv. Manuf. Technol. **62**, 953-63 (2012).

[12] N. Zhao, J. Li, X. Yang J. Mater. Sci. **39**, 4829-34 (2004).

[13] J.A.K. Gladston, N.M. Sheriff, I. Dinaharan, J.D.R. Selvam, Tra. Nonfer. Met. Soc. Chi. **25**, 683-91 (2015).

[14] S.D. Saravanan, M. Senthilkumar, S. Shankar, Tribol. Trans. **56**, 1156-67 (2013). doi: https://doi.org/10.1080/10402004.2013.831962

[15] B.A. Kumar, N. Murugan, Mater. Des. **40**, 52-58 (2012). doi: https://doi.org/10.1016/j.matdes.2012.03.038

[16] K. Antonova, L. Duta, A. Szekeres, G.E. Stan, I.N. Mihailescu, M. Anastasescu, Appl. Surf. Sci. **394**, 197-204 (2017). doi: https://doi.org/10.1016/j.apsusc.2016.10.114

[17] K.M. Lee, D.K. Oh, W.S. Choi, T. Weissgärber, B. Kieback, J. Alloys Compd. **434**, 375-377 (2007). doi: https://doi.org/10.1016/j.jallcom.2006.08.176

[18] S.C. Tjong, G.S. Wang, J. Mater. Sci. **41**, 5263-68 (2006).

[19] M. Kida, L. Weber, C. Monachon, A. Mortensen, J. Appl. Phys. **109**, 064907 (2011).

[20] M. Vetterli, R. Tavangar, L. Weber, A. Scr. Mater. **64** (2), 153-156 (2011). doi: https://doi.org/10.1016/j.scriptamat.2010.09.032

[21] H.C. Hsu, J.Y. Chou, W.H. Tuan, J. Asian Ceram. Soc. **4**, 201-04 (2016).

[22] G.C. Efe, M. Ipek, S. Zeytin, C. Bindal, Comp. Part B: Eng. **43**, 1813-22 (2012).

[23] S. Sheibani, A. Ataie, S. Heshmati-Manesh, Metall. Mater. Trans. A **41**, 2606-12 (2010).

[24] S.C. Tjong, G.S. Wang, J. Mater. Sci. **41**, 5263-68 (2006).

[25] A.S. Sharma, N. Mishra, K. Biswas, B. Basu, Wear **306** (1-2), 138-48 (2013). doi: https://doi.org/10.1016/j.wear.2013.07.009

[26] L.Y. Gu, G.Y. Liang, Z.B. Zheng, J. Mater. Eng. Perform. **16**, 554-58 (2007).

[27] C.S. Ramesh, R.N. Ahmed, M.A. Mujeebu, M.Z. Abdullah, Mater. Des. **30**, 1957-65 (2009).

[28] H. Xing, X. Cao, W. Hu, L. Zhao, J. Zhang, Mater. Lett. **59** (12), 1563-66 (2005). doi: https://doi.org/10.1016/j.matlet.2005.01.023

[29] L. Zhang, X.H. Qu, B.H. Duan, X.B. He, M.L. Qin, L.U. Xin, Trans. Nonferrous Met. Soc. China **18**, 872-78 (2008).

[30] S. Rathod, O.P. Modi, B.K. Prasad, A. Chrysanthou, D. Vallauri, V.P. Deshmukh, Mater. Sci. Eng. A **502**, 91-98 (2009).

[31] J. Lee, N.J. Kim, J.Y. Jung, E.S. Lee, S. Ahn, Scr. Mater. **39**, 1063-69 (1998).

[32] Z.Y. Ma, Metall. Mater. Trans. A **39**, 642-58 (2008).

[33] TitusThankachan, K. SooryaPrakash, V. Kavimani, Comp. Part B: Eng. **174** (2019). https://doi.org/10.1016/j.compositesb.2019.107057Get rights and content

[34] R.S. Mishra, Z.Y. Ma, I. Charit, Mater. Sci. Eng. A **341**, 307-10 (2003).

[35] R. Sathiskumar, N. Murugan, I. Dinaharan, S.J. Vijay, Mater. Des. **55**, 224-234 (2014).

[36] H.R. Akramifard, M. Shamanian, M. Sabbaghian, M. Esmailzadeh, Mater. Des. **54**, 838-844 (2014).

[37] P. Xue, G.M. Xie, B.L. Xiao, Z.Y. Ma, L. Geng, Metall. Mater. Trans. A **41**, 2010-2021 (2010).

[38] H.S. Kim, Mater. Sci.Eng. A **289**, 30-33 (2000).

[39] J.F. Archard, J. Appl. Phys. **24**, 981-988 (1953).

[40] S. Saravanakumar, S. Gopalakrishnan, I. Dinaharan, K. Kalaiselvan, Surf. Coat. Technol. Technology **322**, 51-58 (2017).